Collisional Deactivation of Ba 5d7p $^3D_1$ by Noble Gases†

John E. Smedley,* Sarah K. Coulter, Edward J. Felton, and Kayla S. Zomlefer

Department of Physics and Astronomy, 44 Campus Avenue, Bates College, Lewiston Maine 04240-6084

Received: March 14, 2008; Revised Manuscript Received: May 30, 2008

Collisional deactivation of the 5d7p $^3D_1$ state of Ba by noble gases is studied by time- and wavelength-resolved fluorescence techniques. A pulsed, frequency-doubled dye laser at 273.9 nm excites the 5d7p $^3D_1$ level from the ground state, and fluorescence at 364.1 and 366.6 nm from the 5d7p $^3D_1 \rightarrow$ 6s5d $^3D_1$ and 5d7p $^3D_1 \rightarrow$ 6s5d $^3D_2$ transitions, respectively, is monitored in real time to obtain the deactivation rate constants. At 835 K these rate constants are as follows: He, $(1.69 \pm 0.08) \times 10^{-9}$ cm^3 s^{-1}; Ne, $(3.93 \pm 0.14) \times 10^{-10}$ cm^3 s^{-1}; Ar, $(4.53 \pm 0.15) \times 10^{-10}$ cm^3 s^{-1}; Kr, $(4.64 \pm 0.13) \times 10^{-10}$ cm^3 s^{-1}; Xe, $(5.59 \pm 0.22) \times 10^{-10}$ cm^3 s^{-1}. From time-resolved 5d7p $^3D_1$ emission in the absence of noble gas and from the intercepts of the quenching plots, the lifetime of this state is determined to be 100 ± 1 ns. Using time- and wavelength-resolved Ba emission with a low background pressure of noble gas, radiative lifetimes of several near-resonant states are determined from the exponential rise of the fluorescence signals. These results are as follows: 5d6d $^3D_3$, 28 ± 3 ns; 5d7p $^3P_1$, 46 ± 2 ns; 5d6d $^3G_3$, 21.5 ± 0.8 ns; 5d7p $^3F_3$, 48 ± 1 ns. Integrated fluorescence signals are used to infer the relative rate constants for population transfer from the 5d7p $^3D_1$ state to eleven near-resonant fine structure states.

1. Introduction

Experimental study of alkaline earth−noble gas atom collisions provides useful test cases for the development of theoretical models. Given the two-electron character of alkaline earth atoms and the inaccessibility of excited noble gas states at thermal energies, theoretical investigation of these systems allows close comparison to experiment. A variety of experimental techniques have been applied including cell experiments on the quenching kinetics[1–7] and half-collision dynamics,[8] and beam studies of alignment effects and the spectroscopy of noble gas−alkaline earth diatomic molecules.[9–11] Measurement of fine structure state-changing rate constants, in particular, helps to elucidate atomic interactions in conjunction with the calculation of potential curves and quantum dynamics calculations.

Much of the previous work on Ba has focused on either low-lying excited states or high-lying Rydberg series. Collisional deactivation of 6s6p $^1P_1$ state by noble gases was studied by Breckenridge and Merrow,[10] who reported highly selective transfer to 6s6p $^3P_2$. Brust and Gallagher[7] reported on measurement of excitation transfer rate coefficients between the 6s6p ^3P_J, 6s5d $^1D_2$, and 6s5d ^3D_J levels of Ba. This work was followed by theoretical calculations of barium−helium potentials[12] and close-coupling calculations of the rate coefficients,[13] which showed reasonable agreement with experiment.

The present work is a continuation of a previous study of high-lying excited states of Ba,[1] in which multiple excited states lie within kT of the laser-excited state, leading to multiple pathways for excitation transfer (Figure 1). Both spin-changing and fine structure-changing collisions are observed. Highly excited Ba exists in two types of states, those which are assigned primary configurations that involve one ground-state electron and one excited electron, such as 6snp where $n = 6, 7, 8...$, as well as doubly excited configurations such as Ba 5d^2, 5d7p, etc. For a heavy atom such as Ba these labels cannot be taken too literally, as atomic structure calculations reveal significant configuration mixing.[14] Such is certainly the case for the laser excitation pathway in this study, nominally 6s^2 $^1S_0 \rightarrow$ 5d7p $^3D_1$. Previous studies of Rydberg state spectroscopy in Ba have shown that many levels interact in the highly excited atom.[15,16] Still, there are levels that are predominantly Rydberg in character and others that are predominantly of doubly excited character, and one motivation of the present work is to study how these two types might interact differently in atomic collisions. Such differences may be reflected in total collisional deactivation rates and in specificity of transfer to particular atomic levels.

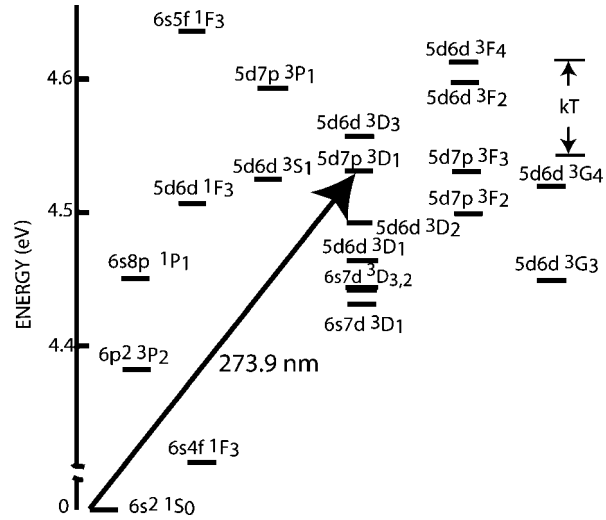

Figure 1. Energy level diagram of the barium atom, indicating excitation at 273.9 nm from the ground state to the 5d7p $^3D_1$ excited state, and near-resonant levels involved in this study.

We have measured the total deactivation rate constants for the 5d7p $^3D_1$ state of barium with each of the noble gases. Collisions cause the initial 5d7p $^3D_1$ population to fan out into a multitude of near resonant states, all of which are indicated

† Part of the "Stephen R. Leone Festschrift".

* Corresponding author. E-mail: jsmedley@bates.edu.

10.1021/jp8022327 CCC: $40.75
Published on Web 07/17/2008

in Figure 1. We observe fluorescence from eleven near-resonant states, and for several of them radiative lifetimes are determined from the exponential rise times of time-resolved double-exponential emission signals. Figure 1 includes all known Ba energy levels within approximately kT (0.072 eV at 835 K) of the 5d7p $^3D_1$ state for completeness, even though we are not able to observe emission from all levels with sufficient signal to include them in this study. In addition we report the radiative lifetime of 5d7p $^3D_1$. By measuring the normalized fluorescence intensity from these near-resonant states and comparing it to the intensity of a 5d7p $^3D_1 \rightarrow$ 6s5d $^1D_2$ emission line, we infer the relative rate constants for individual state-changing collisions. In our kinetic model, absolute state-changing rate constants cannot be determined without knowing the Einstein A coefficients of the individual emission lines, which relate emission intensities to atomic population densities, and the Einstein A coefficient of a transition that originates from 5d7p $^3D_1$, which is typically used to normalize intensities. Even so, relative rate constants give some insight into particularities of the collision dynamics by indicating the noble gas dependence of transfer to individual fine structure states.

2. Experimental Section

The experimental apparatus has been described in detail in a previous work.[1] Briefly, a pulsed Nd:YAG laser pumps a grazing-incidence dye oscillator/amplifier, and the dye output is then frequency-doubled in a beta-barium borate crystal. Laser pulses of approximately 50 microjoules at 273.9 nm are produced in a 2.5 ns pulse at a 10 Hz repetition rate, exciting the 6s^2 $^1S_0 \rightarrow$ 5d7p $^3D_1$ transition. In determining the total deactivation rates, fluorescence from 5d7p $^3D_1$ to both the 6s5d $^3D_1$ and 6s5d $^3D_2$ levels at 364.1 and 366.6 nm, respectively, passes through a 365 nm, 10 nm fwhm bandpass filter before striking an R928 photomultiplier tube. A 175 MHz, 100 MC/s digitizing oscilloscope records the time-resolved signals without amplification. The time-resolved traces are stored on a personal computer for least-squares fitting to a single exponential decay. Inverse lifetimes of these decay curves are plotted as a function of noble gas density and rate constants are determined from the slopes of linear least-squares fits.

Barium metal is housed in the center of a stainless steel cross vacuum cell wrapped with heater wire enclosed in an inconel sheath. Barium vapor is generated and noble gas mixes with the metal vapor through a vacuum manifold maintained by a diffusion pump and cold trap. The UV laser beam is directed through the cell and fluorescence is observed perpendicular to the beam. A chromel−alumel thermocouple is attached to a flange on the arm opposite the fluorescence collection arm and suspended over the region where the laser beam passes through Ba vapor. Noble gas samples have stated purities of at least 99.995% and are used without further purification after pumping and flushing of the connecting lines with high-purity He. Pressures are measured with a capacitance manometer.

Atomic fluorescence signals from the photomultiplier are taken directly into the 50 Ω input of the oscilloscope without amplification. Several experimental checks ensure that the observed signals are linear. Signal levels are kept at about 40 mV or less to ensure a linear response of the photomultiplier, and studies of the lifetime of the 5d7p $^3D_1$ level in pure Ba vapor at constant density are made as a function of signal strength by attenuating the ultraviolet laser beam with an iris diaphragm. The signal is observed to be linear in laser intensity when the intensity is varied by detuning the BBO crystal. At constant laser intensity, the lifetime of the initial state is measured as a function of temperature, and hence barium density, to ensure that radiation trapping is not a significant factor, given the metastable nature of the 6s5d ^3D_J multiplet.[17]

Radiative lifetimes for collisionally populated near resonant states are determined from the exponential risetime of double exponential signals, recorded with a 600 MHz bandwidth, 1 Gigasample per second digitizing oscilloscope, stored on floppy disk and analyzed by least-squares fitting. Spectra are recorded with a pair of boxcar averagers, with gate widths that span the time duration of the transient signals from a pair of photomultiplier tubes. One signal is wavelength resolved with a 0.3 m monochromator, using 15 μm wide slits. A pair of fused silica lenses images the line of laser-excited fluorescence onto the entrance slit, with an intervening pair of aluminum mirrors to rotate the image from a horizontal line to a vertical line that more effectively overlaps the slit. In the fluorescence path and prior to the lens that focuses the emission onto the entrance slit, a fused silica window at approximately 45° to the collimated fluorescence splits off a fraction and sends it to a second photomultiplier tube with the narrowband 365 nm filter, to provide normalization for laser power and barium density fluctuations. Both integrated fluorescence signals are collected on a personal computer, which integrates the area under the spectral lines and ratios the wavelength-resolved signal to the normalizing 365 nm signal. This ratio is the normalized emission intensity, which for each transition is proportional to the rate constant for 5d7p $^3D_1$ transfer to a near resonant fine structure state.

3. Results and Discussion

3.1. Radiative Lifetimes. The basic kinetic model used in this study has been described in detail elsewhere.[1] It assumes that loss of excitation from the manifold of highly excited barium states takes place largely through radiative processes. This essential simplification in the kinetic analysis is possible because all Ba states close in energy to the 5d7p $^3D_1$ level have strongly allowed radiative decay pathways, due to significant configuration mixing. This is evidenced by the observation that the selection rule for J, the total angular momentum, is typically the only parameter determining which transitions are allowed. In the limit of "low" noble gas density, the decay of the barium atom population is largely governed by radiative rates and transfer to near-resonant states through collisions are a small perturbation. If the laser-excited 5d7p $^3D_1$ state is designated as "1", and the near-resonant states are given the index "i", the time-dependent population of the ith state, $n_i(t)$, in the limit of low noble gas density is[1]

$$n_i(t) = \frac{k_{1i} M n_1^0}{\Gamma_i - k_d M - \Gamma_1}\left[e^{-(k_d M + \Gamma_1)t} - e^{-\Gamma_i t}\right]$$

where k_d is the total deactivation rate constant for 5d7p $^3D_1$, Γ_1 is the inverse radiative lifetime of 5d7p $^3D_1$, Γ_i is the inverse radiative lifetime of the ith near-resonant state, M is the noble gas density, n_1^0 is the initial density of 5d7p $^3D_1$ atoms, and k_{1i} is the fine structure changing cross section for population transfer between 5d7p $^3D_1$ and the ith near resonant state. Thus, the time-dependent population of each product state is given by a rising and falling exponential, and the exponential risetime is equal to the radiative lifetime of the near resonant product state, as long as $\Gamma_i > k_d M + \Gamma_1$. All rise times are observed to be significantly shorter than the 100 ns lifetime of the 5d7p state and are thereby identified as radiative lifetimes of the near resonant states populated by collisional transfer.

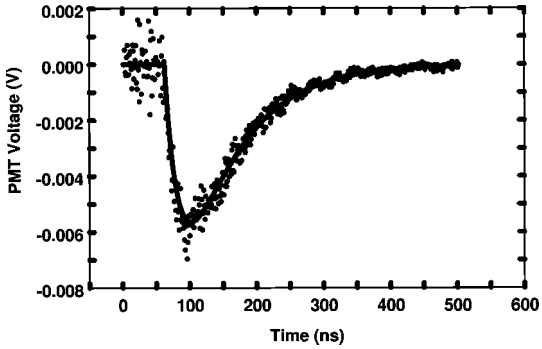

Figure 2. Fluorescence at 746.1 nm from the 5d6d $^3G_4 \rightarrow$ 5d6p $^3F_3$ transition, following transfer from 5d7p $^3D_1$ due to He collision, at 873 K. A least-squares fit to a rising and falling exponential gives a risetime of 21.8 ± 0.9 ns, the radiative lifetime of the 5d6d $^3G_4$ state.

TABLE 1: Radiative Lifetimes of Selected Barium States

λ (nm)	state	τ (ns)
364.1, 366.6	5d7p $^3D_1$	100 ± 1
432.52	5d6d $^3D_3$	28 ± 3
712.04	5d7p $^3P_1$	46 ± 2
746.09	5d6d $^3G_4$	21.5 ± 0.8
767.36	5d7p $^3F_3$	48 ± 1

Several radiative lifetimes are determined in this work by fitting eq 2 to data such as that shown in Figure 2, by the technique described in a previous work.[18] First, a selected time region in the exponential tail of the trace is linear least-squares fit to a decaying exponential. A curve generated from this fit is then back extrapolated and the entire data set is subtracted from it, leaving a "residue" that corresponds to the rising exponential. This residue is then fit to a single exponential to obtain the exponential rate constant for the rising part of the emission signal, and the overall fit to the entire trace is examined. Due to a lack of signal it was not possible to obtain reliable radiative lifetimes for all the near-resonant states, given the difficulty of fitting double exponential shapes for signals with a peak signal-to-noise of less than approximately 5:1. All double exponential fits are checked visually to ensure a good match to the experimental data. One example of an emission that could not be fit to a simple double exponential is the 5d6d $^3S_1 \rightarrow$ 6s6p $^3P_0$ transition at 413.2 nm. Three attempts using different time regions in the least-squares fits produced curves that did not match the data well and gave exponential rise times of 28, 34, and 41 ns. Real time traces of this particular transition have been observed to be very complex at higher temperatures when the Ba density is increased, which may indicate the onset of stimulated emission.

Radiative lifetimes for states whose transitions gave good fits to double exponential curves are listed in Table 1. To our knowledge, this is the first report of these radiative lifetimes. Although numerous Ba Rydberg series have been studied to very high quantum numbers, including doubly excited Rydberg configurations,[19] we are not aware of any atomic structure calculations of these doubly excited states, or calculations of radiative lifetimes and branching ratios.

3.2. Total Deactivation Rate Constants. In the limit of low pressure of noble gas, such that collisions that repopulate the 5d7p $^3D_1$ level are minimized, the time-dependent population density of atoms in the 5d7p state is given by

$$n_1(t) = n_1^0 e^{-[k_d M + \Gamma]t}$$

Here the laser pulse is assumed to be a delta function such that the density of 5d7p ^{3}D1 atoms at $t = 0$ is n_1^0, k_d is the deactivation rate constant, and Γ is the radiative rate of the 5d7p $^3D_1$ state.[1] In the data analysis, time-resolved signals are carefully checked to ensure that single-exponential behavior is observed.

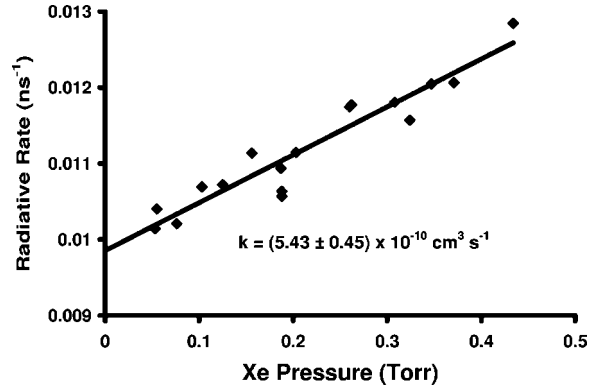

Figure 3. Plot of the radiative decay rate of 5d7p $^3D_1 \rightarrow$ 6s5d $^3D_{1,2}$ emission at 364.1 and 366.6 nm vs Xe pressure, at 835 K. The size of the data points indicates approximately the uncertainty in the decay rate, obtained from a least-squares fit to a single exponential decay. A least-squares straight line fit to the data has a slope of (5.43 ± 0.45) × 10^{-10} cm^3 s^{-1}.

TABLE 2: Deactivation Rate Constants for 5d7p $^3D_1$, all in Units of 10^{-10} cm^3 s^{-1}

	trial 1	trial 2	average
He	16.9 ± 0.8		16.9 ± 0.8
Ne	3.93 ± 0.19	3.94 ± 0.20	3.93 ± 0.14
Ar	4.57 ± 0.16	4.34 ± 0.36	4.53 ± 0.15
Kr	4.63 ± 0.16	4.67 ± 0.24	4.64 ± 0.13
Xe	5.43 ± 0.45	5.64 ± 0.25	5.59 ± 0.22

TABLE 3: Total Average Deactivation Cross Sections for 6s8p $^1P_1$ and 5d7p $^3D_1$ by Noble Gases, in Å^2

	σ_d (6s8p $^1P_1$)[a]	σ_d (5d7p $^3D_1$)
He	210 ± 9	79 ± 4
Ne	72 ± 2	39 ± 1.5
Ar	89 ± 3	60 ± 2
Kr	101 ± 5	80 ± 2
Xe	185 ± 6	109 ± 4

[a] Reference 1.

Inverse lifetimes are plotted vs noble gas density to determine k_d from the slope, as shown for one set of data with Xe as perturber, in Figure 3. Two separate determinations of the rate constants are made on separate days to check the reproducibility of the results, for all noble gases except helium. All of these results are given in Table 2, along with the weighted average of the rate constants from the two linear fits. The zero-pressure intercepts of these plots are in good agreement with each other and with the measured 5d7p $^3D_1$ radiative lifetime in the absence of noble gas. From a weighted average of all the intercepts, the lifetime of the 5d7p $^3D_1$ state is found to be 100 ± 1 ns, where the uncertainty is one standard deviation of the mean.

Average deactivation cross sections for the 5d7p $^3D_1$ state are found by dividing the rate constants by the average relative velocity of the barium−noble gas collision at 835 K. These are listed along with the average deactivation cross sections for the 6s8p $^1P_1$ state, in Table 3, and illustrated in Figure 4. The 6s8p $^1P_1$ results illustrate the basic trend of large rate constant for He and Xe, with a minimum at Ne, as has been observed previously in the case of Ca 4s4p $^1P_1$ transfer[2]. This dependence is analogous to that observed in alkali atom−noble gas atom collisions and follows the trend of free electron scattering by noble gases.[20] In addition, from the previous study of excitation

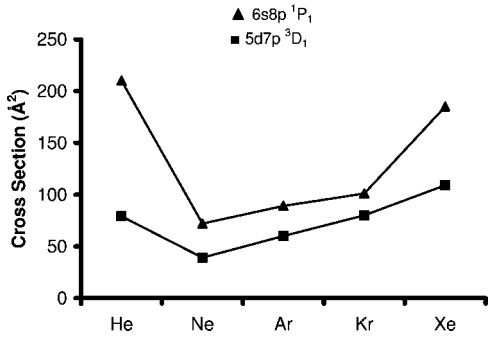

Figure 4. Total deactivation cross section for 6s8p $^1P_1$ (▲) and 5d7p $^3D_1$ (■) in A^2 is plotted as a function of noble gas, indicating an overall similar trend, with significantly larger cross sections for the more Rydberg-like 6s8p state. The 6s8p $^1P_1$ data are from ref 1.

transfer from 6s8p $^1P_1$ the largest state-to-state rate constants occur to the 6s7d ^3D multiplet, suggesting that a simple picture of an 8p → 7d one-electron state change in the collisions has some validity. For He, Ne and Xe the 5d7p $^3D_1$ cross sections are about a factor of 2 smaller than those of 6s8p $^1P_1$, whereas the cross section for Ar is about 33% smaller and for Kr, about 20% smaller. The 5d7p level is at 36495 cm^{-1} whereas the 6s8p state is at 35892 cm^{-1}, and it may be that the difference in quenching cross section is due to the more compact spatial extent of the 5d7p wave function versus that of the 6s8p, although such a claim is qualitative and theoretical studies of the atomic structure, potential curves and dynamics are needed to substantiate it. Cross sections for Kr and Xe, the most polarizable noble gases, are the largest in the case of 5d7p $^3D_1$ and thus the trend in cross section is not identical to that of 6s8p $^1D_1$. This suggests that perhaps a stronger interaction potential leads to more favorable curve crossings for state-changing collisions involving an atom that has more of a doubly excited atomic configuration.

3.3. Spectroscopy of Individual Fine Structure State-Changing Collisions. Wavelength-resolved spectra of the excitation transfer states, properly normalized, can provide rate constants for individual state changing collisions, via

$$k_{1i} = \frac{\Gamma_i}{M}\frac{S_i}{S_1}$$

where k_{1i} is the rate constant for transfer from 5d7p $^3D1$ to state i, M is the noble gas density, and the integrated spectral intensities S_i and S_1 are given by

$$S_i = A_{ik} N_i E F(\lambda_i)$$

where A_{ik} is the Einstein A coefficient between levels i and k, N_i is the time-integrated population density of level i over the width of the boxcar gate, E is an electronics factor that accounts for the boxcar gate, input impedance, and scale setting, and $F(\lambda)$ is an optical detection factor that includes the solid angle of light collection, the transmission/reflection coefficient of the collection optics, the monochromator transmission function and the photomultiplier responsivity.[1] This optical detection factor is determined in a separate set of measurements using a NIST-traceable calibrated lamp. In this expression, S_1 is the integrated intensity of emission from the laser-excited 5d7p $^3D_1$ level. Table 4 lists observed spectral lines, A coefficients, and optical detection factors.

Unfortunately, absolute A_{ik} coefficients are not known for several transitions observed in this work, in particular the emissions from 5d7p $^3D_1$, the laser-excited state, the 5d6d ^3D multiplet, and 5d6d $^1F_3$. However, we can compare the normalized emission intensities *for a particular emission line* as a function of the noble gas perturber. These quantities are proportional to the relative rate constant for transfer from 5d7p $^3D_1$ to a particular fine structure level, as a function of noble gas. Relative rate constants from normalized relative emission intensities, in cases where A coefficients are known, are listed in Table 5, and those gathered from emission lines with unknown A coefficients are listed in Table 6. Duplicate sets of data are presented for the 6p^2 $^1D_2$ level because it is observed separately through two emission lines, corresponding to transitions to the 6s6p $^3P_1$ level at 440.25 nm and the 6s6p $^3P_2$ level at 458.10 nm. The variation in relative rate coefficients for these two data sets in Table 5 is indicative of the large uncertainty in published A coefficients for the two transitions. Across the set of rare gases the trends in rate constants are similar, indicating good agreement between the intensity measurements of the 440.25 and 458.10 nm spectral lines.

All the relative rate constants are represented graphically in Figures 5 and 6, where it can be seen that the rate constants for transfer from 5d7p $^3D_1$ to the different fine structure states show different trends with respect to the noble gas collision partner. For example, a significant contrast in rate constant dependence

TABLE 4: Transitions Used To Determine Relative Rate Constants

λ (nm)	transition	A (10^7 s^{-1})[a]	$F(\lambda)$
408.21	6s8p $^1P_1$ → 6s5d $^1D_2$	0.33	2.76
446.71	5d6d $^3G_3$ → 6s6p $^3P_2$	0.067	3.57
435.03	6p^2 $^3P_2$ → 6s6p $^3P_1$	3.0	3.34
440.25	6p^2 $^1D_2$ → 6s6p $^3P_1$	3.5	3.38
458.10	6p^2 $^1D_2$ → 6s6p $^3P_2$	9.0	3.70
426.44	6s7d $^3D_1$ → 6s6p $^3P_0$	0.75	3.42
449.36	6s7d $^3D_2$ → 6s6p $^3P_2$	1.8	3.64
448.90	6s7d $^3D_3$ → 6s6p $^3P_2$	2.1	3.63

[a] From ref 21.

TABLE 5: Relative Rate Coefficients for Transfer from 5d7p $^3D_1$ to Select States[a]

state	He	Ne	Ar	Kr
6s8p $^1P_1$	1.02	0.27	0.15	0.18
5d6d $^3G_3$	0.36		0.15	0.22
6p$^{23}P_2$	0.065	0.062	0.086	0.035
6p^2 $^1D_2$	0.036	0.0069	0.010	0.012
6p^2 $^1D_2$	0.024	0.0044	0.0079	0.013
6s7d $^3D_1$	0.094	0.027	0.026	0.034
6s7d $^3D_2$	0.075	0.053	0.098	0.105
6s7d $^3D_3$	0.085	0.048	0.076	0.058

[a] Quantities are derived from the normalized, integrated emission intensity of each spectral line, divided by the product of the noble gas density, Einstein A coefficient and the wavelength-dependent spectral detection efficiency. Uncertainties in the integrated intensities are approximately 15%. The A coefficient uncertainties vary from 20% to 50%.

TABLE 6: Relative Rate Coefficients for Transfer from 5d7p $^3D_1$ for Select States for Which Einstein A Coefficients Are Unknown[a]

λ (nm)	state	He	Ne	Ar	Kr
422.51	5d6d $^3D_1$	0.20	0.035	0.055	0.083
440.82	5d6d $^3D_2$	0.32	0.18	0.26	0.15
432.64	5d6d $^3D_3$	0.57	0.29	0.44	0.25
441.50	5d6d $^1F_3$	0.15	0.050	0.063	0.027

[a] Each quantity is derived from the normalized, integrated emission intensity of the spectral line, divided by the noble gas pressure. Uncertainties are approximately 15%.

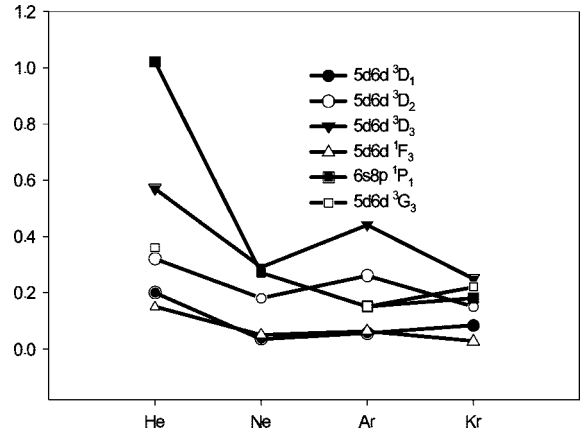

Figure 5. Plots of the relative fine structure changing rate constants, as a function of noble gas collision partner, for six states populated in noble gas−5d7p $^3D_1$ collisions. Comparisons are to be made by following the lines in the figure, which indicate the rate constant dependence on the noble gas partner for a particular fine structure state.

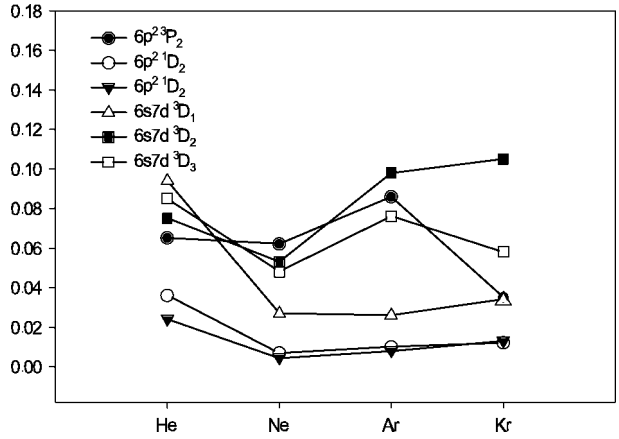

Figure 6. Additional relative fine structure changing rate constants, as a function of noble gas collision partner.

on noble gas collider can be seen by comparing results for 6p^2 $^3P_2$ and 6s7d $^3D_2$ in Figure 6, where the former shows a significant decrease in relative rate constant from Ar to Kr and the latter shows a slight increase. It is curious that the states with the strongest noble gas dependence appear to be 6s8p $^1P_1$ and 6s7d $^3D_1$, in which He is the dominant perturber. Both states nominally appear to be Rydberg in character, although atomic structure calculations are required to substantiate this claim.

We have no detailed explanations for the observed dependencies without knowledge of the relevant potential curves. Brust and Gallagher also noted a significant noble gas perturber dependence in 6s5d $^1D_2 \rightarrow$ 6d5d $^3D_3$ excitation transfer in barium, which they describe as likely due to a radial coupling in the curve crossing between the $^1\Pi_1$ and $^3\Sigma_1$ molecular terms of the barium−noble gas collision complex. Many molecular terms arise from the interaction of noble gases with the energy levels of this study, presenting multiple paths for excitation transfer that can only be sorted out with a firmer knowledge of the interaction potentials.

4. Conclusions and Summary

Total deactivation rate constants for the 5d7p $^3D_1$ state of barium with noble gases have been determined. The magnitudes of the derived cross sections are considerably smaller than those of the 6s8p $^1P_1$ state, although the latter is at somewhat lower energy. In addition, the trend of the total deactivation cross section as a function of noble gas suggests that interesting dynamics are occurring. Radiative lifetimes for several fine structure states in Ba have been determined. Although absolute state-changing cross sections cannot be determined without detailed Einstein *A* coefficients for all the observed spectral lines, relative cross sections for a particular state-changing process show some selectivity with the noble gas perturber and illustrate interesting dynamics. Future studies of state-specific rate constants for 5d7p $^3D_1$ will help more fully to discern the nature of these collisions, as will theoretical determination of the potential curves for noble gas−barium atom pairs.

Acknowledgment. K.Z. was supported by a grant from the Dreyfus foundation. S.K.C. was supported by NSF Research in Undergraduate Institutions grant PHY-9208013. E.F. was supported by a Howard Hughes Medical Institute grant administered by Bates College. Additional support from a William and Flora Hewlett Grant of Research Corp. and from the Donors of the Petroleum Research Fund is gratefully acknowledged.

References and Notes

(1) Smedley, J. E.; Marran, D. F.; Peabody, M. R.; Marquis, C. N. *J. Chem. Phys.* **1993**, *98*, 1093.
(2) Hale, M. O.; Leone, S. R. *J. Chem. Phys.* **1983**, *79*, 3352.
(3) Hale, M. O.; Leone, S. R. *Phys. Rev. A.* **1985**, *31*, 103.
(4) Breckenridge, W. H.; Umemoto, H. *Adv. Chem. Phys.* **1982**, *50*, 325.
(5) Kelly, J. F.; Harris, M.; Gallagher, A. *Phys. Rev. A* **1988**, *37*, 2354.
(6) Chan, Y. C.; Gelbwachs, J. A. *Chem. Phys. Lett.* **1991**, *178*, 523.
(7) Brust, J.; Gallagher, A. C. *Phys. Rev. A* **1995**, *52*, 2120.
(8) Lin, K. C.; Kleiber, P. D.; Wang, J. X.; Stwalley, W. C.; Leone, S. R. *J. Chem. Phys.* **1988**, *89*, 4771.
(9) Kovalenko, L. J.; Robinson, R. L.; Leone, S. R. *J. Chem. Soc., Faraday Trans. 2* **1989**, *85* (8), 939.
(10) Breckenridge, W. H.; Merrow, C. N. J. *Chem. Phys.* **1988**, *88*, 2320.
(11) Kowalski, A.; Funk, D. J.; Breckenridge, W. H. *Chem. Phys. Lett.* **1986**, *132*, 263.
(12) Brust, J.; Greene, C. H. *Phys. Rev. A* **1997**, *56*, 2005.
(13) Brust, J.; Greene, C. H. *Phys. Rev. A* **1997**, *56*, 2013.
(14) Greene, C. H.; Aymar, M. *Phys. Rev. A* **1991**, *44*, 1773.
(15) Hunter, J. E. III.; Keller, J. S.; Berry, R. S. *Phys. Rev. A* **1986**, *33*, 3138.
(16) Armstrong, J. A.; Wynne, J. J.; Esherick, P. *J. Opt. Soc. Am.* **1979**, *69*, 211.
(17) Namiotka, R. K.; Ehrlacher, E.; Sagle, J.; Brewer, M.; Namiotka, D. J.; Hickman, A. P.; Streater, A. D.; Huennekens, J. *Phys. Rev. A* **1996**, *54*, 1996.
(18) Smedley, J. E.; Marran, D. F. *Phys. Rev. A* **1993**, *47*, 126.
(19) Pruvost, L.; Camus, P.; Lecomte, J.-M.; Mahon, C. R.; Pillet, P. *J. Phys. B: At. Mol. Opt. Phys* **1991**, *24*, 4723.
(20) Krause, L. *Adv. Chem. Phys.* **1982**, *28*, 267.
(21) Wiese, W. L.; Martin, G. A. *Natl. Stand. Ref. Data Ser. Natl. Bur. Stand.* **1980**, 68.

JP8022327